Cite as: P. Kongkhambut *et al.*, *Science* 10.1126/science.abo3382 (2022).

# Observation of a continuous time crystal

**Phatthamon Kongkhambut[1], Jim Skulte[1,2], Ludwig Mathey[1,2], Jayson G. Cosme[3], Andreas Hemmerich[1,2]*, Hans Keßler[1]***

[1]Zentrum für Optische Quantentechnologien and Institut für Laser-Physik, Universität Hamburg, 22761 Hamburg, Germany. [2]The Hamburg Center for Ultrafast Imaging, 22761 Hamburg, Germany. [3]National Institute of Physics, University of the Philippines, Diliman, Quezon City 1101, Philippines.

***Corresponding author. Email: hemmerich@physnet.uni-hamburg.de (A.H.); hkessler@physnet.uni-hamburg.de (H.K.)**

**Time crystals are classified as discrete or continuous depending on whether they spontaneously break discrete or continuous time translation symmetry. While discrete time crystals have been extensively studied in periodically driven systems, the experimental realization of a continuous time crystal is still pending. We report the observation of a limit cycle phase in a continuously pumped dissipative atom-cavity system, that is characterized by emergent oscillations in the intracavity photon number. The phase of the oscillation found to be random for different realizations, and hence this dynamical many-body state breaks continuous time translation symmetry spontaneously. Furthermore, the observed limit cycles are robust against temporal perturbations and therefore demonstrate the realization of a continuous time crystal.**

Time crystals are dynamical many-body states that break time translation symmetry in a spontaneous and robust manner (*1*, *2*). The original quantum time crystal envisaged by Frank Wilczek involves a closed many-body system with all-to-all coupling that breaks continuous time translation symmetry by exhibiting oscillatory dynamics in its lowest energy equilibrium state even though the underlying Hamiltonian is time-independent (*1*). This would in fact constitute a startling state of matter in motion, fundamentally protected from bringing this motion to a standstill by energy removal. However, a series of no-go theorems have shown that nature prohibits the realization of such time crystals in isolated systems (*3*–*5*). The search for time crystals was thus extended to include equilibrium scenarios in periodically driven closed systems (*6*–*8*). This has led to realizations of discrete time crystals, which break the discrete time translation symmetry imposed by the external drive (*9*–*17*). In such discrete time crystals, during a short initial phase, the drive slightly excites the system, until the system decouples from the drive, such that further energy or entropy flow is terminated. The system develops a subharmonic response, i.e., an intrinsic oscillation at a frequency slower than that of the drive. Initially, it was argued that dissipation, and hence the use of open systems, must be carefully avoided, until so called dissipative discrete time crystals were theoretically predicted (*18*) and experimentally realized (*19*–*21*). As shown in a number of theoretical works (*22*–*24*), the use of open systems comes with the surprising consequence that continuous instead of periodic driving suffices to induce time crystal dynamics. These continuous time crystals realize the spirit of the original proposal more closely than discrete time crystals and circumvent the no-go theorems via their open character.

Here, we report the observation of a continuous time crystal (CTC) in the form of a limit cycle phase in a continuously pumped dissipative atom-cavity system (Fig. 1A). In classical nonlinear dynamics, the term limit cycle, coined by Poincaré in a mathematical context (*25*), denotes a closed phase space trajectory, asymptotically approached by at least one neighboring trajectory. While limit cycles are well-established in classical nonlinear physics (*26*), there are two essential conditions for limit cycles in open quantum systems to form a CTC. First, the formation of the limit cycle must be associated with spontaneous breaking of continuous time translation symmetry. That is, the relative time phase of the oscillations for repeated realizations takes random values between 0 and $2\pi$. Secondly, the limit cycle phase is robust against temporal perturbations of technical or fundamental character, such as quantum noise and, for open systems, fluctuations associated with dissipation. The characteristic signature of the CTC presented here is a persistent oscillation of the intracavity intensity and atomic density (Fig. 1, B and C), which complies with the robustness and spontaneous symmetry breaking criteria (Fig. 1D).

Our experimental setup consists of a Bose-Einstein condensate (BEC) of $N_a \approx 5 \times 10^4$ $^{87}$Rb atoms inside a high-finesse optical cavity. The system is transversely pumped with a standing wave field with a wavelength $\lambda_p = 792.55$ nm (Fig. 1A). This wavelength is blue detuned with respect to relevant atomic $D_1$ transition of $^{87}$Rb at a wavelength of 794.98 nm. The cavity operates in the recoil resolved regime (*27*), i.e., its field decay rate $\kappa = 2\pi \times 3.4$ kHz is smaller than the recoil frequency $\omega_{rec} = 2\pi \times 3.7$ kHz. The cavity resonance frequency $\omega_c$ is shifted due the the refractive index of the BEC by an amount of $\delta_- = N_a U_0/2$, where $U_0 = 2\pi \times 1.3$ Hz is the maximal light shift per intracavity photon. We define the effective detuning $\delta_{eff} \equiv \delta_c - \delta_-$ where $\delta_c \equiv \omega_p - \omega_c$ is the detuning between the pump field frequency $\omega_p$ and the resonance frequency of the empty cavity $\omega_c$.

Downloaded from https://www.science.org at Staats und Universitaetsbibliothek Hamburg on June 10, 2022

To determine the regime of the CTC, we measure the time dependence of the intracavity photon number $N_P(t)$ that emerges in the protocol given below. We display $N_P(t)$ in Fig. 2A, and two derived quantities, the crystalline fraction $\Xi$, and the limit-cycle frequency $\omega_{LC}$ in Fig. 2, B and C, respectively. In our protocol, the intracavity photon number $N_P(t)$ is recorded as we linearly ramp the pump strength $\varepsilon$ from 0 to 3.5 $E_{rec}$ within 10 ms, while keeping $\delta_{eff}$ fixed. Initially, for weak pump intensities, the BEC phase is stable and $N_P$ is zero. Above a critical value of $\varepsilon$, the BEC becomes unstable toward the formation of a self-organized superradiant phase heralded by a nonzero $N_P$. This represents a many-body state as the cavity photons mediate a retarded infinite-range interaction between the atoms. While this superradiant phase transition has been intensively studied for a red-detuned pump (*28*–*31*), it has only been realized recently for a blue-detuned pump following its theoretical prediction (*32*, *33*). For blue detuning, the atoms are low-field seeking and they localize at the intensity minima of the light field. Nevertheless, the atoms can still self-organize into the superradiant phase as evident from the large blue areas in Fig. 2A. However, the self-organized superradiant phase may become unstable for higher pump strengths, as it costs energy for the atoms to localize away from the nodes of the pump lattice. This behavior leads to the disappearance of the self-organized phase for higher pump strengths (*32*). A phase diagram in fig. S1 in (*34*) shows for a larger range of $\epsilon$, demonstrating the disappearance of the self-organization for strong pumping. In the recoil-resolved regime, due to the retarded character of the cavity-mediated interaction, we additionally observe the emergence of a novel dynamical phase or a limit cycle phase characterized by self-sustained oscillations of $N_P$ as the atoms cycle through different density wave patterns (*33*, *35*). The resolution of the experimental imaging system is insufficient to observe the real space density of the cloud, instead fig. S3 in the supplemental materials shows simulations of the evolution of the single-particle density using a mean-field model. Physically, the limit cycles can be understood as a competition between opposing energy contributions, one coming from the pump lattice potential and another from the cavity-induced all-to-all interaction between the atoms (*33*). In the superradiant phase, the cavity-induced interaction energy dominates and the atoms localize at the antinodes. In the limit cycle phase for sufficiently strong pump intensities, localization of low-field seeking atoms at the antinodes becomes energetically costly, resulting in a decrease in the density modulations and $N_P$ as the system attempts to go back to the normal homogeneous phase. However, this is unstable toward self-organization since the chosen pump strength already exceeds the critical value and thus, the cycle starts anew. The regime of recoil-resolution of the cavity, where the dynamics of the atomic density and the light field evolve with similar time scales, has turned out to be the key ingredient to realize the limit cycle phase. This can be understood by the fact, that the delayed dynamics of the cavity field, with respect to the atomic density, leads to cavity cooling, which in contrast to broadband cavity setups, restricts the atoms to occupy only a small number of momentum modes. This prevents the system from heating up and entering chaotic dynamics. In Fig. 2A, we observe the limit cycle phase in the region enclosed by the yellow dashed lines. To further highlight the dynamical nature of this phase, we show a typical single-shot realization in Fig. 1, B and C.

Next, we quantitatively identify the area in the parameter space, spanned by the pump strength $\varepsilon$ and the effective detuning $\delta_{eff}$, where limit cycles can be observed. For fixed $\delta_{eff}$, we linearly ramp $\varepsilon$ to the desired final value $\varepsilon_f$, using the same slope as for the measurement presented in Fig. 2A, and hold $\varepsilon$ constant for 10 ms. The protocol is depicted by the black curve in Fig. 1B. We show in Fig. 1C an example of the normalized and rescaled single-sided amplitude spectrum $N_P(\omega) = \bar{N}_P(\omega)/\bar{N}_{P,max}(\omega_{LC})$ obtained from $N_P(t)$ within the holding time window [0,10] ms in Fig. 1B. $\bar{N}_P(\omega)$ is the normalized single-sided amplitude spectrum and $\bar{N}_{P,max}(\omega_{LC})$ is the maximum value of the measured limit cycle amplitude. In the case of pronounced limit cycle dynamics as in Fig. 1C, the single-sided amplitude spectrum shows a distinct peak, with a width associated with the limit cycle lifetime of several milliseconds. The narrowest peaks observed exhibit a $e^{-2}$ width $\Delta\omega \approx 2\pi \times 1.4$ kHz: The limit cycle frequency $\omega_{LC}$, plotted in Fig. 2C, is defined as the frequency of the dominant peak in the single-sided amplitude spectrum within the frequency interval $\Delta_{LC} = [3.5,15.5] \times 2\pi$ Hz, chosen much larger than $\delta_{LC} \in [\omega_{LC} - \Delta\omega/2, \omega_{LC} + \Delta\omega/2]$. The oscillation frequency of a CTC is not necessarily fixed and robustness refers to the persistence of the CTC in the thermodynamic limit and for a wide range of system parameters (*22*) (Finite-size effects are discussed in the supplementary materials). We calculate a common measure for time crystallinity, the crystalline fraction $\Xi'$ (*10*, *11*), as the ratio between the area under the single-sided amplitude spectrum within $\delta_{LC}$ and the total area within $\Delta_{LC}$. That is, $\Xi' \equiv \sum_{\omega\in\delta_{LC}} N_P(\omega) / \sum_{\omega\in\Delta_{LC}} N_P(\omega)$. The relative crystalline fraction $\Xi$ shown in Fig. 2B is normalized to the maximum crystalline fraction measured in the parameter space explored in this work. Due to the finite lifetime of the BEC, it is difficult to access the long-time behavior of the system, which makes it experimentally challenging to distinguish between the areas of stable limit cycle, chaos, and possible transient phases. Hence, we define a cut-off or threshold value for the relative crystalline fraction, $\Xi_{cut} = 1/e$, to identify regions with observable limit cycle dynamics. In Fig. 2C, the frequency response of the limit cycle phase is only shown if

Downloaded from https://www.science.org at Staats und Universitaetsbibliothek Hamburg on June 10, 2022

its relative crystalline fraction is higher than the cut-off value, i.e., $\Xi > \Xi_{cut}$. The experimental lifetime of our time crystal is limited by atom loss. Furthermore, the short-range contact interaction, due to collisions between the atoms, leads to dephasing of the system and, hence, melting of the time crystal. Simulations including contact interactions and phenomenological atom loss can be found in the supplementary materials.

The spontaneous symmetry breaking of a many-body system indicates a phase transition. Here, we demonstrate strong evidence that the limit cycle phase emerges through spontaneous breaking of continuous time translation symmetry and thus, it is a CTC. We repeat the experimental protocol used in Fig. 1D for more than 1500 times with fixed $\delta_{eff}/2\pi$ = −5.0 kHz and $\varepsilon_f$ = 1.25 $E_{rec}$. These parameter values are indicated in Fig. 2C by a white cross. Due to technical instabilities, the number of the atoms in the BEC $N_a$ fluctuates by 5%. This leads to a fluctuating value of $\delta_{eff}$ and hence of $\omega_{LC}$. Pictorially, this can be understood by observing that fluctuations in $N_a$ effectively shift the CTC regime in Fig. 2C either up or down. For the parameter values indicated by a white cross in Fig. 2C, the median of $\omega_{LC}$ is $\bar{\omega}_{LC} = 2\pi \times 9.69$ kHz. Our discrete Fourier transform resolution, set by the 10 ms time window, is 100 Hz. Thus, we only consider experimental runs, which yielded response frequencies of $\omega_{LC} = \bar{\omega}_{LC} \pm 2\pi \times$ (50 Hz). For each single-shot measurement, we obtain the time phase defined as the principal argument arg[$N_P(\omega_{LC})$] of the Fourier transformed intracavity photon number $N_P(\omega_{LC})$ evaluated at the limit cycle frequency $\omega_{LC}$. In Fig. 1D, we present the distribution of the observed time phases, which randomly covers the interval [0,2π). This corroborates the spontaneous breaking of continuous time translation symmetry in the limit cycle phase. In the bottom of Fig. 1D we present two specific experimental realizations, which having a time phase difference of almost π. Simulations representing the BEC as a coherent state show a range of the response frequency distribution of 300 Hz. Since we post-select our data far below this limit, the origin of the spread over 2π in the time phase distribution is not due to technical noises but rather due to quantum fluctuations. In the supplementary materials, we show a more detailed theoretical analysis to support this argument. Note that the error bars along the angular direction in Fig. 1D represent the phase uncertainty within 100 Hz of our Fourier limit. The average phase uncertainty is around 0.25π. The uncertainty in the radial direction corresponding to the oscillation amplitude is, however, negligible. Moreover, we remove 30% of the error bars for clarity in Fig. 1D.

Finally, we demonstrate the robustness of the limit cycle phase against temporal perturbations, which is a defining feature of time crystals. We introduce white noise onto the pump signal with a bandwidth of 50 kHz. The noise strength is quantified by $n \equiv \sum_{\omega=0}^{2\pi\times 50\text{kHz}} \left|\mathcal{A}_{\text{noisy}}(\omega)\right| \Big/ \sum_{\omega=0}^{2\pi\times 50\text{kHz}} \left|\mathcal{A}_{\text{clean}}(\omega)\right| - 1$, where $\mathcal{A}_{\text{noisy}}$ ($\mathcal{A}_{\text{clean}}$) is the single-sided amplitude spectrum of the pump in the presence (absence) of white noise. We choose the parameters $\delta_{eff}/2\pi$ = −50 kHz and $\varepsilon_f$ = 1.25 $E_{rec}$ in the center of the stable limit cycle region, indicated by the white cross in Fig. 2C, and add white noise with varying strengths. In the upper panels of Fig. 3, A and B, single-shot realizations of the noisy pump signal are shown for weak and strong noise, respectively. The corresponding dynamics of $N_P$ is shown in the bottom panels of the respective plots. In Fig. 3E, we show how increasing the noise strength can 'melt' the CTC as inferred by the decreasing relative crystalline fractions calculated from single-sided amplitude spectra, similar to those shown in Fig. 3, C and D. Note that the system takes time to react to the noise, such that a few oscillations can always be observed before decay sets in. This leads to an offset of 0.4 in the crystalline fraction even for very strong noise. Nevertheless, we find that the limit cycle phase indeed exhibits robust oscillatory behavior over a wide range of the noise strength. This, together with the observation of spontaneous breaking of a continuous time translation symmetry, suggests that the observed limit cycle phase is a CTC.

In conclusion, we have experimentally demonstrated a continuous time crystal, and provided a theoretical understanding. This class of dynamical many-body states expands the concepts of long-range order and spontaneous symmetry breaking into the time domain, and is therefore of fundamental interest. This result, and the exquisite precision and control achieved with our atom-cavity platform, paves the way toward a broad and comprehensive study of dynamical many-body states of bosonic or fermionic quantum matter in the strongly correlated regime. For example, an increased atom-photon coupling could generate a new class of time crystals associated with symmetry broken periodic entanglement. Furthermore, technological applications, e.g., toward time metrology, can be envisioned.

## REFERENCES AND NOTES


1. F. Wilczek, Quantum time crystals. *Phys. Rev. Lett.* **109**, 160401 (2012). doi:10.1103/PhysRevLett.109.160401 Medline
2. A. Shapere, F. Wilczek, Classical time crystals. *Phys. Rev. Lett.* **109**, 160402 (2012). doi:10.1103/PhysRevLett.109.160402 Medline
3. P. Nozières, EPL. *Europhys. Lett.* **103**, 57008 (2013).
4. P. Bruno, Impossibility of spontaneously rotating time crystals: A no-go theorem. *Phys. Rev. Lett.* **111**, 070402 (2013). doi:10.1103/PhysRevLett.111.070402 Medline
5. H. Watanabe, M. Oshikawa, Absence of Quantum Time Crystals. *Phys. Rev. Lett.* **114**, 251603 (2015). doi:10.1103/PhysRevLett.114.251603 Medline
6. D. V. Else, C. Monroe, C. Nayak, N. Y. Yao, Discrete Time Crystals. *Annu. Rev. Condens. Matter Phys.* **11**, 467–499 (2020). doi:10.1146/annurev-conmatphys-031119-050658
7. K. Sacha, *Time Crystals* (Springer, Cham, 2020).


Downloaded from https://www.science.org at Staats und Universitaetsbibliothek Hamburg on June 10, 2022

8. V. Khemani, R. Moessner, S. L. Sondhi, A brief history of time crystals. arXiv:1910.10745 [cond-mat.str-el] (2019).
9. J. Zhang, P. W. Hess, A. Kyprianidis, P. Becker, A. Lee, J. Smith, G. Pagano, I.-D. Potirniche, A. C. Potter, A. Vishwanath, N. Y. Yao, C. Monroe, Observation of a discrete time crystal. *Nature* **543**, 217–220 (2017). doi:10.1038/nature21413 Medline
10. S. Choi, J. Choi, R. Landig, G. Kucsko, H. Zhou, J. Isoya, F. Jelezko, S. Onoda, H. Sumiya, V. Khemani, C. von Keyserlingk, N. Y. Yao, E. Demler, M. D. Lukin, Observation of discrete time-crystalline order in a disordered dipolar many-body system. *Nature* **543**, 221–225 (2017). doi:10.1038/nature21426 Medline
11. J. Rovny, R. L. Blum, S. E. Barrett, Observation of Discrete-Time-Crystal Signatures in an Ordered Dipolar Many-Body System. *Phys. Rev. Lett.* **120**, 180603 (2018). doi:10.1103/PhysRevLett.120.180603 Medline
12. J. Smits, L. Liao, H. T. C. Stoof, P. van der Straten, Observation of a Space-Time Crystal in a Superfluid Quantum Gas. *Phys. Rev. Lett.* **121**, 185301 (2018). doi:10.1103/PhysRevLett.121.185301 Medline
13. S. Autti, V. B. Eltsov, G. E. Volovik, Observation of a Time Quasicrystal and Its Transition to a Superfluid Time Crystal. *Phys. Rev. Lett.* **120**, 215301 (2018). doi:10.1103/PhysRevLett.120.215301 Medline
14. J. O'Sullivan *et al.*, *New J. Phys.* **22**, 085001 (2020).
15. A. Kyprianidis, F. Machado, W. Morong, P. Becker, K. S. Collins, D. V. Else, L. Feng, P. W. Hess, C. Nayak, G. Pagano, N. Y. Yao, C. Monroe, Observation of a prethermal discrete time crystal. *Science* **372**, 1192–1196 (2021). doi:10.1126/science.abg8102 Medline
16. J. Randall, C. E. Bradley, F. V. van der Gronden, A. Galicia, M. H. Abobeih, M. Markham, D. J. Twitchen, F. Machado, N. Y. Yao, T. H. Taminiau, Many-body-localized discrete time crystal with a programmable spin-based quantum simulator. *Science* **374**, 1474–1478 (2021). doi:10.1126/science.abk0603 Medline
17. X. Mi, M. Ippoliti, C. Quintana, A. Greene, Z. Chen, J. Gross, F. Arute, K. Arya, J. Atalaya, R. Babbush, J. C. Bardin, J. Basso, A. Bengtsson, A. Bilmes, A. Bourassa, L. Brill, M. Broughton, B. B. Buckley, D. A. Buell, B. Burkett, N. Bushnell, B. Chiaro, R. Collins, W. Courtney, D. Debroy, S. Demura, A. R. Derk, A. Dunsworth, D. Eppens, C. Erickson, E. Farhi, A. G. Fowler, B. Foxen, C. Gidney, M. Giustina, M. P. Harrigan, S. D. Harrington, J. Hilton, A. Ho, S. Hong, T. Huang, A. Huff, W. J. Huggins, L. B. Ioffe, S. V. Isakov, J. Iveland, E. Jeffrey, Z. Jiang, C. Jones, D. Kafri, T. Khattar, S. Kim, A. Kitaev, P. V. Klimov, A. N. Korotkov, F. Kostritsa, D. Landhuis, P. Laptev, J. Lee, K. Lee, A. Locharla, E. Lucero, O. Martin, J. R. McClean, T. McCourt, M. McEwen, K. C. Miao, M. Mohseni, S. Montazeri, W. Mruczkiewicz, O. Naaman, M. Neeley, C. Neill, M. Newman, M. Y. Niu, T. E. O'Brien, A. Opremcak, E. Ostby, B. Pato, A. Petukhov, N. C. Rubin, D. Sank, K. J. Satzinger, V. Shvarts, Y. Su, D. Strain, M. Szalay, M. D. Trevithick, B. Villalonga, T. White, Z. J. Yao, P. Yeh, J. Yoo, A. Zalcman, H. Neven, S. Boixo, V. Smelyanskiy, A. Megrant, J. Kelly, Y. Chen, S. L. Sondhi, R. Moessner, K. Kechedzhi, V. Khemani, P. Roushan, Time-crystalline eigenstate order on a quantum processor. *Nature* **601**, 531–536 (2022). doi:10.1038/s41586-021-04257-w Medline
18. Z. Gong, R. Hamazaki, M. Ueda, Discrete Time-Crystalline Order in Cavity and Circuit QED Systems. *Phys. Rev. Lett.* **120**, 040404 (2018). doi:10.1103/PhysRevLett.120.040404 Medline
19. H. Keßler, P. Kongkhambut, C. Georges, L. Mathey, J. G. Cosme, A. Hemmerich, Observation of a Dissipative Time Crystal. *Phys. Rev. Lett.* **127**, 043602 (2021). doi:10.1103/PhysRevLett.127.043602 Medline
20. P. Kongkhambut, H. Keßler, J. Skulte, L. Mathey, J. G. Cosme, A. Hemmerich, Realization of a Periodically Driven Open Three-Level Dicke Model. *Phys. Rev. Lett.* **127**, 253601 (2021). doi:10.1103/PhysRevLett.127.253601 Medline
21. H. Taheri, A. B. Matsko, L. Maleki, K. Sacha, All-optical dissipative discrete time crystals. *Nat. Commun.* **13**, 848 (2022). doi:10.1038/s41467-022-28462-x Medline
22. F. Iemini, A. Russomanno, J. Keeling, M. Schirò, M. Dalmonte, R. Fazio, Boundary Time Crystals. *Phys. Rev. Lett.* **121**, 035301 (2018). doi:10.1103/PhysRevLett.121.035301 Medline
23. B. Buča, J. Tindall, D. Jaksch, Non-stationary coherent quantum many-body dynamics through dissipation. *Nat. Commun.* **10**, 1730 (2019). doi:10.1038/s41467-019-09757-y Medline
24. H. Keßler, J. G. Cosme, M. Hemmerling, L. Mathey, A. Hemmerich, Emergent limit cycles and time crystal dynamics in an atom-cavity system. *Phys. Rev. A* **99**, 053605 (2019). doi:10.1103/PhysRevA.99.053605
25. H. Poincaré, *J. Math. Pures Appl.* **7**, 375 (1881).
26. S. H. Strogatz, *Nonlinear Dynamics and Chaos: With Applications to Physics, Biology, Chemistry, and Engineering* Westview press (2015).
27. H. Keßler, J. Klinder, M. Wolke, A. Hemmerich, Optomechanical atom-cavity interaction in the sub-recoil regime. *New J. Phys.* **16**, 053008 (2014). doi:10.1088/1367-2630/16/5/053008
28. P. Domokos, H. Ritsch, Collective cooling and self-organization of atoms in a cavity. *Phys. Rev. Lett.* **89**, 253003 (2002). doi:10.1103/PhysRevLett.89.253003 Medline
29. A. T. Black, H. W. Chan, V. Vuletić, Observation of collective friction forces due to spatial self-organization of atoms: From Rayleigh to Bragg scattering. *Phys. Rev. Lett.* **91**, 203001 (2003). doi:10.1103/PhysRevLett.91.203001 Medline
30. K. Baumann, C. Guerlin, F. Brennecke, T. Esslinger, Dicke quantum phase transition with a superfluid gas in an optical cavity. *Nature* **464**, 1301–1306 (2010). doi:10.1038/nature09009 Medline
31. J. Klinder, H. Keßler, M. Wolke, L. Mathey, A. Hemmerich, Dynamical phase transition in the open Dicke model. *Proc. Natl. Acad. Sci. U.S.A.* **112**, 3290–3295 (2015). doi:10.1073/pnas.1417132112 Medline
32. P. Zupancic, D. Dreon, X. Li, A. Baumgärtner, A. Morales, W. Zheng, N. R. Cooper, T. Esslinger, T. Donner, P-Band Induced Self-Organization and Dynamics with Repulsively Driven Ultracold Atoms in an Optical Cavity. *Phys. Rev. Lett.* **123**, 233601 (2019). doi:10.1103/PhysRevLett.123.233601 Medline
33. F. Piazza, H. Ritsch, Self-Ordered Limit Cycles, Chaos, and Phase Slippage with a Superfluid inside an Optical Resonator. *Phys. Rev. Lett.* **115**, 163601 (2015). doi:10.1103/PhysRevLett.115.163601 Medline
34. Supplementary text is available in the supplementary materials.
35. H. Keßler, J. G. Cosme, C. Georges, L. Mathey, A. Hemmerich, From a continuous to a discrete time crystal in a dissipative atom-cavity system. *New J. Phys.* **22**, 085002 (2020). doi:10.1088/1367-2630/ab9fc0
36. P. Kongkhambut *et al.*, Data for "'Observation of a continuous time crystal". Zenodo (2022); doi:10.5281/zenodo.6576125.
37. A. Polkovnikov, Phase space representation of quantum dynamics. *Ann. Phys.* **325**, 1790–1852 (2010). doi:10.1016/j.aop.2010.02.006
38. J. G. Cosme, J. Skulte, L. Mathey, Time crystals in a shaken atom-cavity system. *Phys. Rev. A* **100**, 053615 (2019). doi:10.1103/PhysRevA.100.053615

## ACKNOWLEDGMENTS

H.K. thanks J. Klinder and C. Georges for helpful discussions and their support. J.G.C. thanks R. J. L. Tuquero for valuable insights and discussions. A.H. acknowledges useful discussions with C. Zimmermann and J. Marino. **Funding:** This work is funded by the Deutsche Forschungsgemeinschaft (DFG, German Research Foundation) through grant DFG-KE2481/1–1. P.K., J.S., L.M. and A.H. acknowledge the DFG for funding through SFB-925 – project 170620586, and the Cluster of Excellence "Advanced Imaging of Matter" (EXC 2056) – project No. 390715994. J.S. acknowledges support from the German Academic Scholarship Foundation. **Author contributions:** P.K. and H.K. performed the experiments and data analysis. The simulations were performed by J.S. and J.G.C., supported by L.M.. The project was designed and supervised by H.K. and A.H.. All authors contributed to the discussion and interpretation of the results, as well as, to writing the manuscript. **Competing interests:** The authors declare no competing interests. **Data and materials availability:** All data presented in this paper and simulation scripts are deposited at Zenodo (*36*). **License information:** Copyright © 2022 the authors, some rights reserved; exclusive licensee American Association for the Advancement of Science. No claim to original US government works. https://www.science.org/about/science-licenses-journal-article-reuse

Downloaded from https://www.science.org at Staats und Universitaetsbibliothek Hamburg on June 10, 2022

**SUPPLEMENTARY MATERIALS**
science.org/doi/10.1126/science.abo3382
Materials and Methods
Supplementary Text
Figs. S1 to S7
References (*37*, *38*)

Submitted 14 February 2022; accepted 25 May 2022
Published online 9 June 2022
10.1126/science.abo3382

Downloaded from https://www.science.org at Staats und Universitaetsbibliothek Hamburg on June 10, 2022

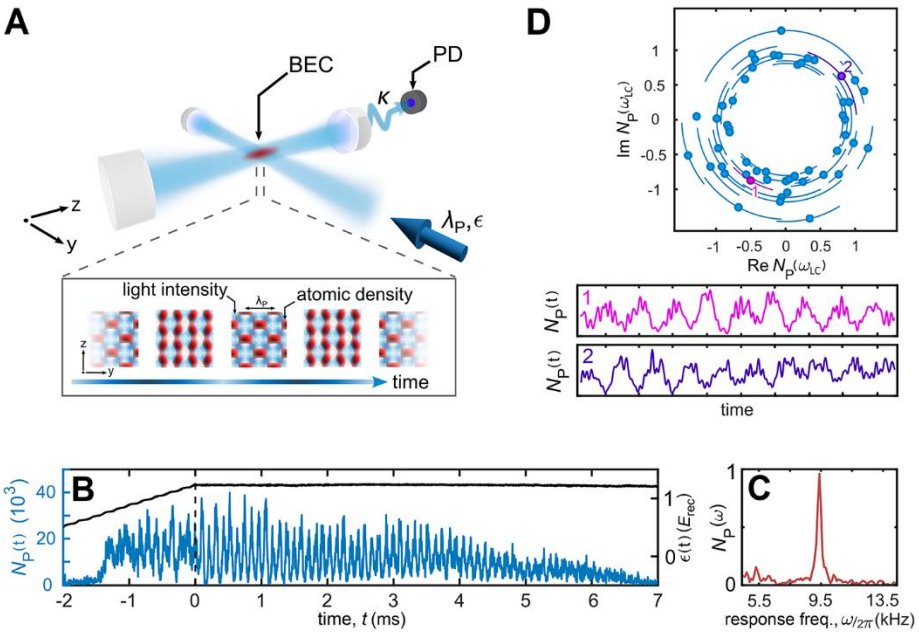


**Fig. 1. Continuous time crystal in an atom-cavity system.** (**A**) Schematic drawing of the atom-cavity system pumped transversely with an optical pump lattice, blue detuned with respect to an atomic transition. The inset in the bottom shows the photon field (blue) and the atomic density (red) of the limit cycle dynamics, based on simulations. The blue color shading of the time axis indicates the intracavity photon number. (**B**) Single experimental realization of the limit cycle phase for $\delta_{eff}/2\pi = -3.8$ kHz and $\varepsilon_f = 1.25E_{rec}$. The vertical dashed black line indicates the start of the 10 ms holding time, wherein the pump strength is held constant. Black line: time trace of the pump strength $\varepsilon$. Blue line: time evolution of the intracavity photon number $N_P(t)$. (**C**) Normalized and rescaled single-sided amplitude spectrum of $N_P$ calculated from the data shown in (B). (**D**) Distribution of the time phase in the limit cycle phase for $\delta_{eff}/2\pi = -5.0$ kHz and $\varepsilon_f = 1.25E_{rec}$. The error bars represent the phase uncertainty within our discrete Fourier transform resolution of 100 Hz. The uncertainty with regard to the radial dimension, i.e., the amplitude uncertainty, however, is negligibly small. For clarity, we remove the errors bars, around 30%, which are overlapping. The two panels in the bottom show the evolution of the intracavity photon number for two specific experimental realizations, marked with 1,2 the upper panel, which have a time phase difference of almost π.

Downloaded from https://www.science.org at Staats und Universitaetsbibliothek Hamburg on June 10, 2022

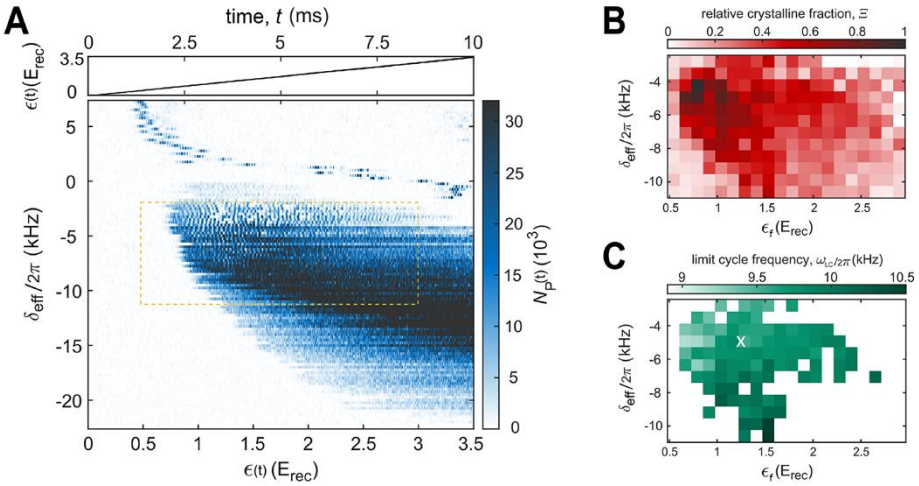


**Fig. 2. Determining the time-crystalline regime.** (**A**) Top panel: Pump strength protocol. Bottom panel: The corresponding intracavity photon number $N_P$ as a function of $\delta_{eff}$ and $\varepsilon$. The area enclosed by the yellow dashed lines marks the parameter space spanned in B and C. (**B**) Relative crystalline fraction $\Xi$ and (**C**) limit cycle frequency $\omega_{LC}$ plotted versus $\delta_{eff}$ and $\varepsilon_f$. To obtain B and C, for fixed $\delta_{eff}$, the pump strength is ramped to its final value $\varepsilon_f$, and subsequently held constant for 10 ms. The relative crystalline fraction $\Xi$ and the corresponding value of $\omega_{LC}$ to identify the time-crystalline state. The parameter space is divided into 20 × 24 plaquettes and averages over 5 to 10 experimental implementations are produced. The white cross indicates the parameter values $\delta_{eff}/2\pi = -5.0$ kHz and $\varepsilon_f = 1.25E_{rec}$. The white area in C corresponds to data with $\Xi$ below $1/e$.

Downloaded from https://www.science.org at Staats und Universitaetsbibliothek Hamburg on June 10, 2022

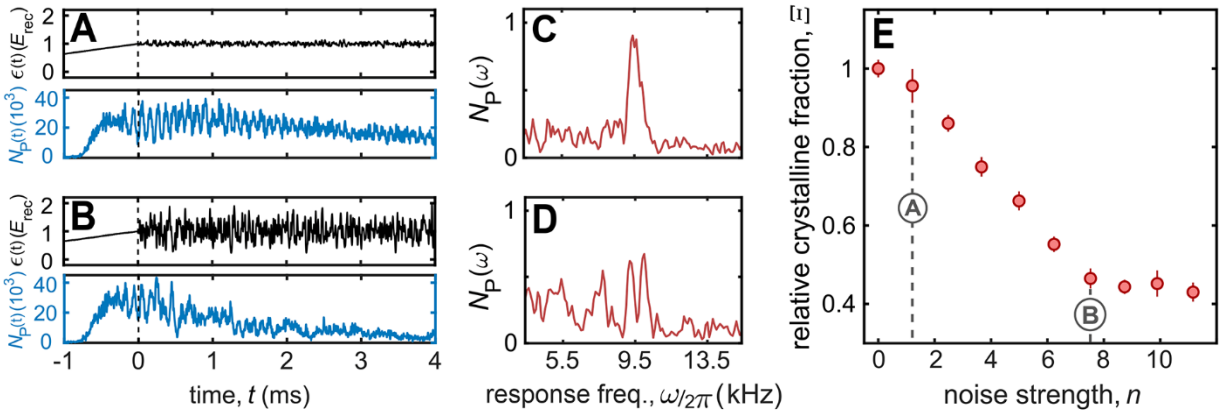


Fig. 3. Robustness against temporal perturbations. (A and B) Single experimental runs for noise strengths indicated in (E). Top panels: time traces of the pump strength $\varepsilon$. Bottom panel: corresponding dynamics of $N_P$. (C and D) Single-sided amplitude spectra of (A) and (B), respectively. (E) Relative crystalline fraction for varying noise strength $n$ and fixed $\delta_{eff}/2\pi = -5.0$ kHz and $\varepsilon_f = 1.25E_{rec}$.

Downloaded from https://www.science.org at Staats und Universitaetsbibliothek Hamburg on June 10, 2022

Science

# Observation of a continuous time crystal

Phatthamon KongkhambutJim SkulteLudwig MatheyJayson G. CosmeAndreas HemmerichHans Keßler

*Science*, **Ahead of Print** • DOI: 10.1126/science.abo3382

**View the article online**
https://www.science.org/doi/10.1126/science.abo3382
**Permissions**
https://www.science.org/help/reprints-and-permissions

Downloaded from https://www.science.org at Staats und Universitaetsbibliothek Hamburg on June 10, 2022

Use of this article is subject to the Terms of service

*Science* (ISSN ) is published by the American Association for the Advancement of Science. 1200 New York Avenue NW, Washington, DC 20005. The title *Science* is a registered trademark of AAAS.
Copyright © 2022 The Authors, some rights reserved; exclusive licensee American Association for the Advancement of Science. No claim to original U.S. Government Works